Improving numerical snowpack simulations by assimilating land surface temperature.

Esteban Alonso-González[1], Simon Gascoin[1], Sara Arioli[2], Ghislain Picard[2]

[1]Centre d'Etudes Spatiales de la Biosphère, Université de Toulouse,CNRS/CNES/IRD/INRA/UPS, Toulouse, France
[2]Univ. Grenoble Alpes, CNRS, Institut des Géosciences de l'Environnement (IGE), Grenoble, France

Correspondence: Alonso-Gonzalez E.: esteban.alonso-gonzalez@univ-tlse3.fr

Abstract. The assimilation of data from Earth observation satellites into numerical models is considered as the path forward to estimate SWE distribution in mountain catchments. The land surface temperature (LST) can be observed from space, but its potential to improve SWE simulations remains underexplored. This is likely due to the insufficient temporal or spatial resolution offered by the current thermal infrared (TIR) missions. However, three planned missions will provide global-scale TIR data at much higher spatio-temporal resolution in the coming years.

To investigate the value of TIR data to improve SWE estimation, we developed a synthetic data assimilation experiment at five snow-dominated sites covering a latitudinal gradient in the northern hemisphere. We generated synthetic true LST and SWE series by forcing an energy-balance snowpack model with the ERA5-Land reanalysis. We used this synthetic true LST to recover the synthetic true SWE from a degraded version of ERA5-Land. We defined different observation scenarios to emulate the revisiting times of Landsat 8 (16 days) and the Thermal infraRed Imaging Satellite for High-resolution Natural resource Assessment (TRISHNA) (3 days), while accounting for cloud cover. We replicated the experiments 100 times at each experimental site to assess the robustness of the assimilation process. We performed the assimilation using two different approaches: a sequential scheme (particle filter) and a smoother (particle batch smoother).

The results show that LST data assimilation using the smoother reduced the normalized Root Mean Square Error (nRMSE) of the simulations from 57% (open loop) to 7% and 3% for 16 day revisit and 3 day revisit respectively, in the absence of clouds. We found similar but higher nRMSE values by removing observations due to cloud cover but with a substantial increase of the standard deviation of the nRMSE of the replicates, highlighting the importance of revisiting times in the stability of the assimilation output. The smoother largely outperformed the particle filter algorithm, suggesting that the capability of a smoother to propagate the information along the season is key to exploit LST information for snow modeling. These results suggest that the LST data assimilation has an underappreciated potential to improve snowpack simulations and highlight the value of upcoming TIR missions to advance snow hydrology.

1 Introduction

The seasonal snowpack plays a key role in many ecological and hydrological processes worldwide (Barnett et al., 2005).
Due to its high albedo and insulating capabilities, the extensive snow-covered area of the northern hemisphere influences the
Earth climate system (Henderson et al., 2018). In mountain regions, the seasonal snowpack is also an important source of
runoff during the summer when the water demand peaks. Hence, an accurate knowledge of the snowpack conditions has an
important economic value (Sturm et al., 2017). The snow cover is also a source of natural hazards such as floods caused by
rain-on-snow events or snow avalanches, events that are expected to increase due to the impacts of climate warming
(Ballesteros-Cánovas et al., 2018; Musselman et al., 2018).

Despite its importance, monitoring the snowpack remains challenging for both scientists and water management agencies.
The variable nature of the snowpack makes it difficult to deploy and maintain ground based snow monitoring networks
(Kinar & Pomeroy, 2015). Therefore, snow hydrologists have developed methods to take advantage of satellite remote
sensing since the beginning of the Landsat programme (Rango & Martinec, 1979). Yet, the application of remote sensing in
snow hydrology remains hindered by the lack of direct observations of the snow water equivalent (SWE) in mountain
regions (Dozier et al., 2016).

Numerical models allow simulating many snowpack state variables, including the SWE. However, their accuracy is
constrained by the large uncertainty of the meteorological forcing (Raleigh et al., 2015). Recent studies suggest that data
assimilation (DA) of remotely sensed products is the path forward to estimate the spatial distribution of relevant snowpack
characteristics (Aalstad et al., 2018; Charrois et al., 2016; Cortés & Margulis, 2017; Margulis et al., 2016; Smyth et al.,
2020; Stigter et al., 2017). Using DA techniques it is possible to fuse model simulations and multiple remote sensing datasets
to improve the snowpack simulations. In particular, the snow cover area was assimilated in many case studies due to its
widespread availability (e.g. Baba et al., 2018, Alonso-González et al., 2021). Yet, the extent of the snow cover provides no
direct information on the internal state of the snowpack and is blind to snowpack changes when the pixel is fully snow
covered.

The ice-surface temperature (IST), is a key state variable for simulating the snowpack evolution. Physically-based snowpack
models solve the energy balance equation iteratively along the time dimension, estimating the IST at each timestep of the
model (Essery, 2015; Liston & Elder, 2006). Also it is a key parameter to estimate the emitted energy as outgoing longwave
radiation .The estimation of the IST allows forecasting the occurrence of the melting events, as when the IST reaches 0°C all
the added energy is converted to melt. Thus, assimilating IST may provide key information about the timing of the melting
events. Also, the assimilation of the land surface temperature (LST) (i.e. the temperature of the earth surface independently if
it is snow covered) may improve the snowpack simulations by different mechanisms. The IST is physically bound to the
melting point temperature, while once the snow melts, the LST can exceed 0°C. Thus the assimilation of the LST may
indirectly provide information of the snow cover area too. Also, it should be possible to improve the snow simulations by
retrieving thermal information when there is no sunlight, like during the night time or during the polar night at high latitudes.

A previous study showed that IST DA improved the surface ice mass balance simulations of the Greenland ice sheet (Navari et al., 2016), fusing IST stimations with the CROCUS snow model. On the other hand, previous research suggested little improvements in the mass simulations after assimilating LST simulations retrieved from the Meteosat Second Generation (MSG) (~6km spatial resolution) in the Alps. However, the coarse resolution of the LST products of MSG prevents use in complex terrain, and more research is needed to assess the potential of high resolution LST DA.

The thermal imagery already available only offers coarse resolution for the snow applications over complex terrain (MODIS, Sentinel-3) or long revisiting times (Landsat). This has probably prevented the study of the impact of LST DA, although recent research suggests that LST can provide useful information to retrieve internal snowpack properties (Colombo et al., 2019), a capability that can be exploited from satellites (Colombo et al., 2023). The availability of high spatiotemporal resolution LST products will be improved in the short term with the appearance of new satellites, such as the French-Indian mission Thermal infraRed Imaging Satellite for High-resolution Natural resource Assessment (TRISHNA) (Lagouarde et al., 2018). TRISHNA is expected to provide surface temperature measurements at 60 m spatial resolutions every 3 days. Also, given the agenda of the space agencies high resolution thermal infrared retrievals will be readily accessible in the near future. For instance the LSTM (Copernicus Land Surface Temperature Monitoring) (Koetz et al., 2018) which will offer similar observations as TRISHNA but with improved spectral, spatial and temporal resolutions and the SBG satellite (Surface Biology and Geology)(Cawse-Nicholson et al., 2021) from NASA which will provide similar high resolution TIR images of the surface of the earth. The combination of these three missions may eventually provide close to bi-daily (day and night time) high resolution thermal infrared observations of the earth surface. In this context the objectives of this work are; i) to test the potential of the LST to improve the snowpack simulations and ii) explore the effect of increasing the temporal observations.

A convenient approach to emulate future remote sensing observations is to use an Observing System Simulation Experiment (OSSE). For example, Navari et al. (2016) assessed the feasibility to integrate ice surface temperatures in a regional climate model estimate of Greenland ice sheet surface mass balance through an OSSE. Synthetic experiments were also used to explore the potential of data assimilation techniques in improving the snowpack simulations (Clark et al., 2006; Revuelto et al., 2021; Smyth et al., 2019, Deschamps-Berger et al., 2022).

Here, we designed an OSSE to evaluate the benefit of future remote sensing LST to simulate seasonal SWE. In this experiment, synthetic LST and SWE data were generated in several climatic regions. Synthetic LST data were assimilated into a snowpack model under different cloud cover scenarios and satellite revisit times. The benefit of assimilating LST was studied by comparing the posterior SWE to the synthetic SWE.

2 Data and methods

We selected five sites in snow-dominated regions of Europe, spanning 40° of latitude from the Pyrenees mountains to the Svalbard archipelago. The sites were chosen every 10° of latitude approximately to sample different climatic influences .

The southern sites (Gerlachovský štít, Bigorre) are located in high mountain regions (Pyrenees, Tatra), Finse is located on a high elevation plateau (Hardangervidda), whereas Tromsø and Ny-Ålesund are near sea level. Gerlachovský štít is in the Eastern Europe and its climate is influenced by its continental characteristics, Tromsø and Ny-Ålesund exhibit obvious polar climates and Bigorre shows a montane climate with Mediterranean influences.

Table 1: Geographical coordinates and elevation (m a.s.l.) of the ERA5-Land centroids used in the study

Centroid	Longitude	Latitude	Elevation
Ny-Ålesund	12.0°	78.9°	124
Tromsø	19.8°	69.5°	647
Finse	07.5°	60.6°	147
Gerlachovský štít	20.2°	49.2°	1479
Bigorre	00.1°	42.9°	1843

We used ERA5-land surface reanalysis data (Muñoz-Sabater et al., 2021) to force the Flexible Snow Model (FSM2) (Essery, 2015) over four consecutive hydrological years from 01/Sep/2017 to 31/Aug/2021. From this simulation, we retrieved the SWE and LST time series, which were considered as the synthetic truth. The LST was exported at 13:00 local time, corresponding to foreseen TRISHNA overpass time. To mimic instrumental noise, we added to the LST time series a Gaussian noise with a zero mean and a standard deviation of 1.5 K. This standard deviation was chosen as an intermediate value between the reported RMSE of errors obtained by the comparison of Landsat 8 with in situ measurements of the snow surface temperature (RMSE = 2.0 °K) (Robledano et al., 2022) and the expected performance of LST products delivered by the TRISHNA mission (Lagouarde et al., 2018).

The synthetic LST time series were downsampled with a period of 16 and 3 days, to emulate revisit times of Landsat 8 and TRISHNA respectively. We simulated the impact of cloud cover by further removing values in the synthetic LST time series at random dates selected from an uniform distribution. We defined four different cloud cover scenarios with probabilities of 0%, 25%, 50% and 75%.

For each site, we created a new, degraded meteorological forcing to run FSM2 by averaging ERA5-Land data from the nearest 9 cells (i.e. resampling the spatial resolution from 10 km to 30 km approximately). We further perturbed the precipitation field after aggregation using a multiplicative factor of 0.5. This strong perturbation was chosen to emulate precipitation biases that are typically found in global reanalyses and large scale precipitation products (Beck et al., 2019) potentially leading to large underestimation of SWE in mountain regions (Wrzesien et al., 2019). A similar value was already used in previous synthetic snow data assimilation experiment (Deschamps-Berger et al., 2022).

The degraded meteorological forcing and synthetic LST were used to feed the Multiple Snow data Assimilation system (MuSA). MuSA is an open source ensemble based data assimilation toolbox built around the FSM2 model (Alonso-González et al., 2022). We used the same initial conditions to run FSM2 within MuSA (soil temperature profile, initial LST and absence of snow), therefore we did not perform a spin-up. The assimilation experiments were done using the Particle Batch Smoother (PBS) (Margulis et al., 2015). Smoother algorithms are typically used to develop reanalyses as the whole time series of information are available, whereas filtering is rather used for operational forecasting where future observations respective to the analysis step are not available (Largeron et al., 2020). A description of these algorithms and the MuSA toolbox can be found in Alonso-González et al., (2022).

The prior ensemble of FSM2 simulations was composed of 300 particles that were generated by perturbing the air temperature (additive perturbation) and the precipitation (multiplicative perturbation). The perturbations were time-invariant and randomly drawn from a normal distribution of mean $\mu = 0$ and standard deviation $\sigma = 2$ (temperature) and a log-normal distribution with mean $\mu = 0.45$ and standard deviation $\sigma = 0.8$ of the underlying normal distribution (precipitation). These parameters were chosen to cover the expected differences between the "truth" forcing and the degraded forcing and were obtained by preliminary trial and error tests.

While the PF performs the analysis sequentially, i.e. each time an observation occurs, the PBS is a smoother, hence it assimilates all the available observations in a single time window, propagating information from the observations forward and backward in time. Here the assimilation time window was defined as a hydrological year (i.e. one snow season). In both the PF and PBS, prior weights of ensemble members (particles) are updated based on the likelihood, i.e. a measure of the distance between the predictions of each particle and the observations. The posterior weights are then used to estimate posterior statistics from the ensemble, typically its weighted mean and weighted standard deviation. In the case of the PF, we used the bootstrap resampling algorithm to eliminate particles with low weights and replicate particles with high weights by sampling with replacement randomly from the probability distribution of the updated weights. To prevent the filter from collapsing (all the weight is shared by few and eventually just one particle), new perturbation parameters were drawn from a normal approximation of the posterior from the previous analysis step at each new analysis step, instead of resampling both the states of the model and the parameters. A rigorous description of the algorithms, the underlying theory and implementation details can be found in Alonso-González et al., (2022).

For each site and each cloud cover scenario, we ran MuSA and generated a posterior SWE. However, the output of MuSA is stochastic due to the random generation of the forcing perturbation parameters. Also the position of the gaps in the different cloud cover scenarios and the gaussian noise are random. Therefore, to increase the statistical robustness of our results, we repeated each assimilation experiment 100 times, drawing new gaps and gaussian noise for each replicate of the experiment. This created an ensemble of posterior SWE which was compared to the synthetic true SWE.

In total, for a given site, MuSA was run 1600 times (100 replicates x 4 cloud cover scenarios x 2 revisit times x 2 DA algorithms). This corresponds to 480,000 FSM2 runs (300 particles by MuSA run), summing up to 2,400,000 FSM2 runs considering the 5 study areas.

3 Results

As expected, the degradation of the ERA5-Land meteorological forcing had a large impact on the open loop SWE simulations (Fig. 2). In comparison with the true SWE, the average normalized RMSE (nRMSE) was 57% (after removing

155 the summer time months of July and August). The aggregation of the data from neighboring ERA5-Land cells and the scaling of the precipitation caused an overall reduction in the simulated SWE, leading to a shorter snow seasons at all sites (Fig. 2). However, the LST assimilation with the PBS substantially improved the SWE simulations (Fig. 2). This improvement was evident at both revisit times, although the 3 day revisit scenario (nRMSE = 3%) outperformed the 16 day revisit scenario (nRMSE = 7%).

160 The posterior SWE series in Figure 2 were averaged from an ensemble of 100 replicates (see Sect. 2. Data and methods). Figure 3 shows every posterior SWE realization in the case of the Tromsø site under different cloud cover scenarios when assimilating LST at 3-day resolution. This Figure shows that the spread of the posterior ensemble increased with the cloud cover probability. The standard deviation of the obtained nRMSE values over each cloud cover scenario ranged from 1% to 7% in this particular case.

165 Figure 4 summarizes the results of the PBS from all experiments under every cloud cover and revisit scenarios. In all cases, the data assimilation significantly reduced the nRMSE in comparison with the open loop simulations. The nRMSE was always higher for the 16-day revisit compared to the 3-day revisit, but the difference was more pronounced under the 50% and 75% cloud cover scenarios. In addition, the standard deviation of the nRMSE of the 100 replicates was higher for the 16-day compared to the 3-day revisit scenarios. Both the averaged nRMSE and standard deviations increased with the cloud

170 cover with an average nRMSE for all the sites ranging between 3% and 8% in the case of the 3-day revisit experiments and 7% and 22% for the 16-day revisit experiments.

Figure 5 shows the distribution of the mean of the posterior precipitation perturbation parameters obtained from the 100 data assimilation runs using the PBS. It demonstrates that the assimilation of LST reduced the error on the precipitation forcing, since the posterior parameter distributions intersect the actual perturbation factor of 2 that was used to degrade the input

175 precipitation. However, the difference between the true precipitation and the degraded precipitation may not exactly equal to the scaling factor of 2 since the precipitation forcing was also perturbed by aggregating precipitation from the surrounding ERA5-Land cells (Sect. 2). As observed above in Figure 4, the standard deviation of the posterior perturbation parameters of the replicates increased when comparing the 3-day with the 16-day revisit scenarios, as well as with the cloud cover probability.

180 Whereas the above results show that the PBS algorithm clearly improved the SWE simulation, it was not the case with the PF. Figure 6 summarizes the results of the same experiments shown in Figure 4, but using the PF instead of the PBS. In this case the improvement in the average nRMSE of the posterior simulations was not as obvious with respect to the open loop as

in the PBS experiments. Although, in most cases the nRMSE showed a moderate improvement compared with the open loop
on average, several runs among the 100 replicates had a higher nRMSE than the open loop run. The revisit or cloud cover
185 scenarios had no clear effect on the nRMSE. As in the PBS case, there was no significant difference between the different
locations, except for Ny-Ålesund which yielded a higher nRMSE standard deviation than for the other locations. This is a
consequence of the very cold conditions in this polar region, as some particles became "glaciers" due to the perturbed
forcing (non zero SWE at the end of the hydrological year).

4 Discussion

190 Navari et al. (2016) showed the potential of IST data assimilation to improve the surface mass balance of the Greenland ice
sheet in a regional climate simulation with an Ensemble batch smoother. Our study also suggests that the assimilation of LST
can improve seasonal snow simulations in sites with different climate contexts. With the PBS, the improvement was
substantial independently of the site, i.e. the climatic context did not exhibit an obvious influence on the results. However,
our results with the PF also supports the conclusions of Piazzi et al. (2019), who did not obtain obvious improvements in the
195 posterior SWE simulations after assimilating LST using an Ensemble Kalman Filter.Therefore, our study provide an
explanation of the contrasting performances found by Navari et al. (2016) and Piazzi et al. (2019).While Navari et al. (2016)
used smoothers, Piazzi et al. (2019) used a filter. A filter updates the simulations sequentially while smoothers update the
whole season in batch. This in-batch assimilation allows the propagation of the information of the observations backwards in
the simulation. The saw tooth pattern reported by Piazzi et al. (2019) is reminiscent of dynamical inconsistencies associated
200 with filters (Dunne & Entekhabi, 2005). Also, the performance of the LST data assimilation reported by Piazzi et al. (2019)
was probably hampered by the coarse resolution of the MSG LST products that were used to update snowpack simulations at
the point scale. In the specific case of the LST, considering the observations of the whole snow season in a batch may be key
to have a positive impact on the posterior SWE. The trajectory of the LST in seasonal snow dominated regions exhibits a
characteristic pattern as the physical bounds of the IST are different from the LST. Once the snow melts, the LST can rise
205 above the water melting point and therefore the trajectory of the LST may be a good indicator of the length of the snow
season. However, this should not be the only reason, as Navari et al. (2016) experiments were developed over the Greenland
ice sheet where there is a permanent ice cover. During the melting season the IST is fixed to the melting point temperature,
providing information on the duration of the melting period. Also the occurrence of winter time melt events should be visible
in the TIR domain. The information of the whole seasonal trajectory of the LST is propagated to the posterior by using a
210 soother, but not by using a filter. This is highlighted at the Ny-Ålesund site, where the polar conditions made snowmelt
impossible at the end of the hydrological year for some of the replicates leading to very high nRMSE using the PF. These
results suggest that the LST may be less beneficial to snowmelt forecasting applications where the use of filters is more
extended to update the model as new observations arise, but it should be valuable information to improve snow reanalyses
which aim to reconstruct snow cover climatologies.

215 Our results also suggest that even the currently available thermal infrared estimations of the LST from Landsat missions
      have the potential to significantly improve SWE simulations despite a revisit time of 16 days. The emulated revisiting times
      of both Landsat and TRISHNA are the expected values at the equator, and can be lower in other latitudes. Here we did not
      study the effect of the spatial resolution but hypothesized that high resolution (i.e. Landsat-like) is needed for snow cover
      simulations in the studied regions. Landsat TIR images have a 100 m resolution which makes them suitable to sample the
220 slope scale in mountain terrain, hence homogeneous conditions in the energy balance budget (Baba et al., 2019). Despite the
      low revisiting times of the Landsat mission, Landsat TIR imagery may be useful to improve SWE simulations using a
      smoother data assimilation algorithm, an approach that to our knowledge has not been explored yet. More research should be
      carried out on this topic, especially in the context of joint assimilation experiments where more than one variable is
      assimilated.

225

      Nevertheless, the change in revisit from 3 to 16 days in our experiments translated into an approximate doubling of the
      posterior nRMSE. Therefore, we expect significant progress with TRISHNA observations, not to mention the enhanced
      spatial resolution (approximately 60 m). The benefit of the 3 day revisit was particularly evident under 50% to 75% cloud
      cover. This should be considered, as previous global estimates of the cloud cover suggest values closer to our highest cloud
230 cover scenario (Wylie et al., 2005). For instance, cloud cover probability in MODIS products reached 60% in the Alps and
      50% in the Pyrenees (Gascoin et al., 2015; Parajka & Blöschl, 2008).
      In any case, under both revisit scenarios, the cloud cover decreased the precision of the replicates of the posterior SWE, i.e.
      the variability between repeated experiments, but the average was only marginally affected. In other words, the cloud cover
      reduced the robustness of the data assimilation, but even regions with a persistent cloud cover could benefit from LST
235 assimilation. The different replicates of each experiment exhibited different results, with a variance that increased with the
      number of gaps introduced in the synthetic LST observations, suggesting that not all the combinations of observations are
      equally informative. This was also obvious regarding the posterior precipitation perturbation parameters, as the standard
      deviation of the different replicates increased with the percentage of cloud cover.
      Despite the promising potential of the LST to improve SWE simulation, some limitations of the current study inherent to the
240 synthetic nature of the OSSE should be taken into consideration. The use of the same model to generate the real synthetic
      SWE and for the assimilation processes avoids the uncertainty as a consequence of the model internal parameters and
      structural uncertainty. This simplifies the interpretation of the results of our work, but needs to be taken into account in real-
      world scenarios. The simulation of the cloud cover scenarios was generated by selecting random dates from an uniform
      distribution. However, in some regions the cloud cover exhibits marked seasonal patterns (Sudmanns et al., 2020), that may
245 challenge to update the snowpack simulations even with smoothers if cloud cover is more frequent during key periods in the
      snow season.

5 Conclusions

The motivation of this study on LST data assimilation is the upcoming launch of high resolution thermal infrared spatial missions with improved revisit time in the next few years. We implemented a synthetic data assimilation experiment to study

250   the potential of the LST in improving SWE simulations along a latitudinal gradient in the northern hemisphere. The methodology was based on the generation of synthetic LST estimations and SWE true estimates, and a prior ensemble of SWE simulations generated by forcing the FSM2 model with degraded meteorological fields. The MuSA snow data assimilation software was used to generate SWE posterior time series using the particle batch smoother and particle filter algorithms to be compared with synthetic true SWE.

255   The results suggest that the assimilation of LST has a great potential to improve seasonal snowpack simulations across all the tested sites. Gap-free LST series, improved the average nRMSE of the open loop simulations from 57% to 7% and 3% for the 16 days and 3 day revisiting times respectively. However, a lower revisit frequency caused an increase in the variance of the nRMSE when the runs are replicated 100 times, meaning that the assimilation becomes less robust. This conclusion was more evident with high cloud cover scenarios, highlighting the importance of the revisit time in thermal infrared remote

260   sensing to reduce the uncertainty on the updated SWE.

The type of data assimilation was also key to explain the role of LST in improving SWE simulations. The particle batch smoother strongly improved the simulations, whereas the particle filter was much less performant and could even cause a degradation of the simulations at a cold polar site.

Overall, our results encourage a more systematic use of the current LST products within snow data assimilation studies,

265   especially if the objective is to perform a snow reanalysis which can benefit from observations acquired over an entire snow season.

Acknowledgements

This work was supported by the Centre National d'Etudes Spatiales (CNES) through the postdoctoral grant of Esteban Alonso-González, the PhD grant of Sara Arioli and the TOSCA program.

270   **Code and data availability.**

The MuSA code is available at github.com/ealonsogzl/MuSA. The original FSM2 code is found at github.com/RichardEssery/FSM2, and in the MuSA repository with slight modifications from the original versionERA5-Land data is available for download from the Copernicus Climate Data Store.

275

Author contributions. Conceptualization: EAG, SG. Data curation: EAG. Formal analysis: EAG, SG, SA, GP. Funding acquisition: EAG, SG. Investigation: EAG, SG. Methodology: EAG. Project administration: EAG, SG. Resources:EAG, SG. Software: EAG. Supervision: SG, GP. Validation: EAG. Visualization: EAG. Writing - original draft preparation: EAG . Writing review & editing: EAG, SG, SA, GP.

280

Competing interests. The authors declare that they have no conflict of interest.

References

Aalstad, K., Westermann, S., Schuler, T. V., Boike, J., & Bertino, L. (2018). Ensemble-based assimilation of fractional snow-covered area satellite retrievals to estimate the snow distribution at Arctic sites. Cryosphere, 12(1), 247–270.

285   https://doi.org/10.5194/tc-12-247-2018

Alonso-González, E., Gutmann, E., Aalstad, K., Fayad, A., Bouchet, M., & Gascoin, S. (2021). Snowpack dynamics in the Lebanese mountains from quasi-dynamically downscaled ERA5 reanalysis updated by assimilating remotely sensed fractional snow-covered area. Hydrology and Earth System Sciences, 25(8), 4455–4471. https://doi.org/10.5194/hess-25-4455-2021

290   Alonso-González, Esteban, Aalstad, K., Baba, M. W., Revuelto, J., López-Moreno, J. I., Fiddes, J., et al. (2022). MuSA: The Multiscale Snow Data Assimilation System (v1.0). Geoscientific Model Development Discussions, 1–43. https://doi.org/10.5194/gmd-2022-137

Baba, M. W., Gascoin, S., & Hanich, L. (2018). Assimilation of Sentinel-2 data into a snowpack model in the High Atlas of Morocco. Remote Sensing, 10(12), 1982. https://doi.org/10.3390/rs10121982

295   Baba, M. W., Gascoin, S., Kinnard, C., Marchane, A., & Hanich, L. (2019). Effect of Digital Elevation Model Resolution on the Simulation of the Snow Cover Evolution in the High Atlas. Water Resources Research, 55(7), 5360–5378. https://doi.org/10.1029/2018WR023789

Ballesteros-Cánovas, J. A., Trappmann, D., Madrigal-González, J., Eckert, N., & Stoffel, M. (2018). Climate warming enhances snow avalanche risk in the Western Himalayas. Proceedings of the National Academy of Sciences of the United

300   States of America, 115(13), 3410–3415. https://doi.org/10.1073/pnas.1716913115

Barnett, T. P., Adam, J. C., & Lettenmaier, D. P. (2005). Potential impacts of a warming climate on water availability in snow-dominated regions. Nature, 438(7066), 303–309. https://doi.org/10.1038/nature04141

Beck, H. E., Pan, M., Roy, T., Weedon, G. P., Pappenberger, F., van Dijk, A. I. J. M., et al. (2019). Daily evaluation of 26 precipitation datasets using Stage-IV gauge-radar data for the CONUS. Hydrology and Earth System Sciences, 23(1), 207–

305   224. https://doi.org/10.5194/hess-23-207-2019

Cawse-Nicholson, K., Townsend, P. A., Schimel, D., Assiri, A. M., Blake, P. L., Buongiorno, M. F., et al. (2021). NASA's surface biology and geology designated observable: A perspective on surface imaging algorithms. Remote Sensing of Environment, 257, 112349. https://doi.org/10.1016/j.rse.2021.112349

Charrois, L., Cosme, E., Dumont, M., Lafaysse, M., Morin, S., Libois, Q., & Picard, G. (2016). On the assimilation of optical reflectances and snow depth observations into a detailed snowpack model. Cryosphere, 10(3), 1021–1038. https://doi.org/10.5194/tc-10-1021-2016

Clark, M. P., Slater, A. G., Barrett, A. P., Hay, L. E., McCabe, G. J., Rajagopalan, B., & Leavesley, G. H. (2006). Assimilation of snow covered area information into hydrologic and land-surface models. Advances in Water Resources, 29(8), 1209–1221. https://doi.org/10.1016/j.advwatres.2005.10.001

Colombo, R., Garzonio, R., Di Mauro, B., Dumont, M., Tuzet, F., Cogliati, S., et al. (2019). Introducing Thermal Inertia for Monitoring Snowmelt Processes With Remote Sensing. Geophysical Research Letters, 46(8), 4308–4319. https://doi.org/10.1029/2019GL082193

Colombo, Roberto, Pennati, G., Pozzi, G., Garzonio, R., Di Mauro, B., Giardino, C., et al. (2023). Mapping snow density through thermal inertia observations. Remote Sensing of Environment, 284, 113323. https://doi.org/10.1016/j.rse.2022.113323

Cortés, G., & Margulis, S. (2017). Impacts of El Niño and La Niña on interannual snow accumulation in the Andes: Results from a high-resolution 31 year reanalysis: El Niño Effects on Andes Snow. Geophysical Research Letters, 44(13), 6859–6867. https://doi.org/10.1002/2017GL073826

Deschamps-Berger, C., Cluzet, B., Dumont, M., Lafaysse, M., Berthier, E., Fanise, P., & Gascoin, S. (2022). Improving the Spatial Distribution of Snow Cover Simulations by Assimilation of Satellite Stereoscopic Imagery. Water Resources Research, 58(3), e2021WR030271. https://doi.org/10.1029/2021WR030271

Dozier, J., Bair, E. H., & Davis, R. E. (2016). Estimating the spatial distribution of snow water equivalent in the world's mountains. Wiley Interdisciplinary Reviews: Water, n/a-n/a. https://doi.org/10.1002/wat2.1140

Dunne, S., & Entekhabi, D. (2005). An ensemble-based reanalysis approach to land data assimilation. Water Resources Research, 41(2). https://doi.org/10.1029/2004WR003449

Essery, R. (2015). A factorial snowpack model (FSM 1.0). Geoscientific Model Development, 8(12), 3867–3876. https://doi.org/10.5194/gmd-8-3867-2015

Gascoin, S., Hagolle, O., Huc, M., Jarlan, L., Dejoux, J. F., Szczypta, C., et al. (2015). A snow cover climatology for the Pyrenees from MODIS snow products. Hydrology and Earth System Sciences, 19(5), 2337–2351. https://doi.org/10.5194/hess-19-2337-2015

Henderson, G. R., Peings, Y., Furtado, J. C., & Kushner, P. J. (2018). Snow–atmosphere coupling in the Northern Hemisphere. Nature Climate Change, 8(11), 954–963. https://doi.org/10.1038/s41558-018-0295-6

Kinar, N. J., & Pomeroy, J. W. (2015). Measurement of the physical properties of the snowpack. Reviews of Geophysics, 53(2), 481–544. https://doi.org/10.1002/2015RG000481

340   Koetz, B., Bastiaanssen, W., Berger, M., Defourney, P., Del Bello, U., Drusch, M., et al. (2018). High Spatio- Temporal Resolution Land Surface Temperature Mission - a Copernicus Candidate Mission in Support of Agricultural Monitoring. In IGARSS 2018 - 2018 IEEE International Geoscience and Remote Sensing Symposium (pp. 8160–8162). https://doi.org/10.1109/IGARSS.2018.8517433

Lagouarde, J.-, Bhattacharya, B. K., Crébassol, P., Gamet, P., Babu, S. S., Boulet, G., et al. (2018). The Indian-French

345   Trishna Mission: Earth Observation in the Thermal Infrared with High Spatio-Temporal Resolution (pp. 4078–4081). Presented at the IGARSS 2018 - 2018 IEEE International Geoscience and Remote Sensing Symposium. https://doi.org/10.1109/IGARSS.2018.8518720

Largeron, C., Dumont, M., Morin, S., Boone, A., Lafaysse, M., Metref, S., et al. (2020). Toward Snow Cover Estimation in Mountainous Areas Using Modern Data Assimilation Methods: A Review. Frontiers in Earth Science, 8. Retrieved from

350   https://www.frontiersin.org/article/10.3389/feart.2020.00325

Liston, G. E., & Elder, K. (2006). A distributed snow-evolution modeling system (snowmodel). Journal of Hydrometeorology, 7(6), 1259–1276. https://doi.org/10.1175/JHM548.1

Margulis, S. A., Girotto, M., Cortés, G., & Durand, M. (2015). A particle batch smoother approach to snow water equivalent estimation. Journal of Hydrometeorology, 16(4), 1752–1772. https://doi.org/10.1175/JHM-D-14-0177.1

355   Margulis, S. A., Cortés, G., Girotto, M., & Durand, M. (2016). A landsat-era Sierra Nevada snow reanalysis (1985-2015). Journal of Hydrometeorology, 17(4), 1203–1221. https://doi.org/10.1175/JHM-D-15-0177.1

Muñoz-Sabater, J., Dutra, E., Agustí-Panareda, A., Albergel, C., Arduini, G., Balsamo, G., et al. (2021). ERA5-Land: A state-of-the-art global reanalysis dataset for land applications. Earth System Science Data, 13(9), 4349–4383. https://doi.org/10.5194/essd-13-4349-2021

360   Musselman, K. N., Lehner, F., Ikeda, K., Clark, M. P., Prein, A. F., Liu, C., et al. (2018). Projected increases and shifts in rain-on-snow flood risk over western North America. Nature Climate Change, 8(9), 808–812. https://doi.org/10.1038/s41558-018-0236-4

Navari, M., Margulis, S. A., Bateni, S. M., Tedesco, M., Alexander, P., & Fettweis, X. (2016). Feasibility of improving a priori regional climate model estimates of Greenland ice sheet surface mass loss through assimilation of measured ice

365   surface temperatures. The Cryosphere, 10(1), 103–120. https://doi.org/10.5194/tc-10-103-2016

Parajka, J., & Blöschl, G. (2008). Spatio-temporal combination of MODIS images - Potential for snow cover mapping. Water Resources Research, 44(3). https://doi.org/10.1029/2007WR006204

Piazzi, G., Campo, L., Gabellani, S., Castelli, F., Cremonese, E., Cella, U. M. di, et al. (2019). An Enkf-Based Scheme for Snow Multivariable Data Assimilation at an Alpine Site. Journal of Hydrology and Hydromechanics, 67(1), 4–19.

370   https://doi.org/10.2478/johh-2018-0013

Raleigh, M. S., Lundquist, J. D., & Clark, M. P. (2015). Exploring the impact of forcing error characteristics on physically based snow simulations within a global sensitivity analysis framework. Hydrology and Earth System Sciences, 19(7), 3153–3179. https://doi.org/10.5194/hess-19-3153-2015

Rango, A., & Martinec, J. (1979). Application of a Snowmelt-Runoff Model Using Landsat Data. Nordic Hydrology, 10(4),
375   225–238. https://doi.org/10.2166/nh.1979.0006

Revuelto, J., Cluzet, B., Duran, N., Fructus, M., Lafaysse, M., Cosme, E., & Dumont, M. (2021). Assimilation of surface
reflectance in snow simulations: Impact on bulk snow variables. Journal of Hydrology, 603, 126966.
https://doi.org/10.1016/j.jhydrol.2021.126966

Robledano, A., Picard, G., Arnaud, L., Larue, F., & Ollivier, I. (2022). Modelling surface temperature and radiation budget
380   of snow-covered complex terrain. The Cryosphere, 16(2), 559–579. https://doi.org/10.5194/tc-16-559-2022

Smyth, E. J., Raleigh, M. S., & Small, E. E. (2019). Particle Filter Data Assimilation of Monthly Snow Depth Observations
Improves   Estimation   of   Snow   Density   and   SWE.   Water   Resources   Research,   55(2),   1296–1311.
https://doi.org/10.1029/2018WR023400

Smyth, E. J., Raleigh, M. S., & Small, E. E. (2020). Improving SWE Estimation With Data Assimilation: The Influence of
385   Snow   Depth   Observation   Timing   and   Uncertainty.   Water   Resources   Research,   56(5).
https://doi.org/10.1029/2019WR026853

Stigter, E. E., Wanders, N., Saloranta, T. M., Shea, J. M., Bierkens, M. F. P., & Immerzeel, W. W. (2017). Assimilation of
snow cover and snow depth into a snow model to estimate snow water equivalent and snowmelt runoff in a Himalayan
catchment. The Cryosphere, 11(4), 1647–1664. https://doi.org/10.5194/tc-11-1647-2017

390   Sturm, M., Goldstein, M. A., & Parr, C. (2017). Water and life from snow: A trillion dollar science question.

Sudmanns, M., Tiede, D., Augustin, H., & Lang, S. (2020). Assessing global Sentinel-2 coverage dynamics and data
availability for operational Earth observation (EO) applications using the EO-Compass. International Journal of Digital
Earth, 13(7), 768–784. https://doi.org/10.1080/17538947.2019.1572799

Wrzesien, M. L., Pavelsky, T. M., Durand, M. T., Dozier, J., & Lundquist, J. D. (2019). Characterizing Biases in Mountain
395   Snow   Accumulation   From   Global   Data   Sets.   Water   Resources   Research,   55(11),   9873–9891.
https://doi.org/10.1029/2019WR025350

Wylie, D., Jackson, D. L., Menzel, W. P., & Bates, J. J. (2005). Trends in Global Cloud Cover in Two Decades of HIRS
Observations. Journal of Climate, 18(15), 3021–3031. https://doi.org/10.1175/JCLI3461.1

400

405
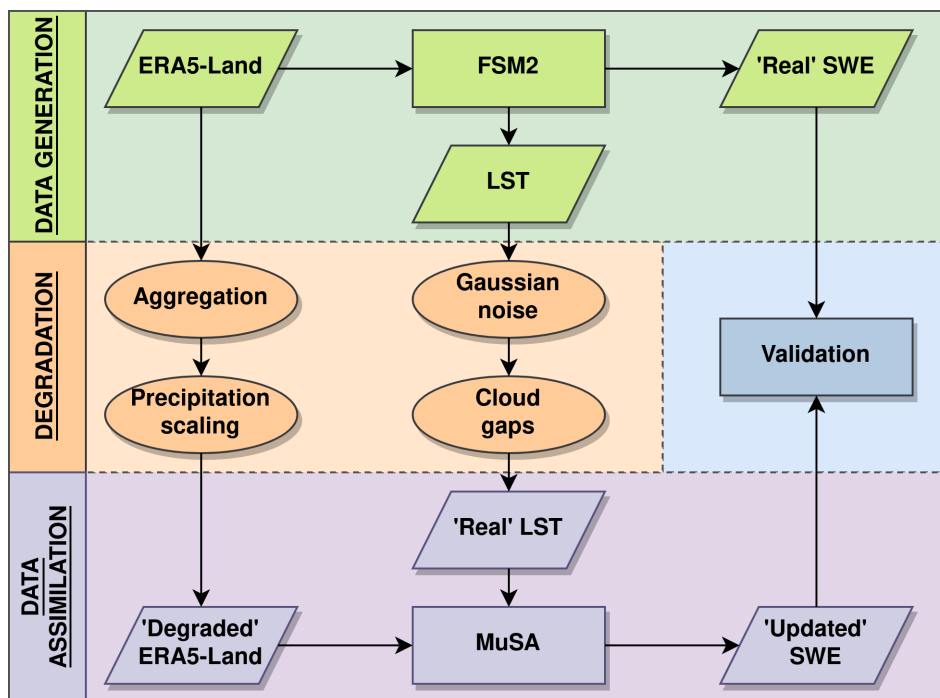
Figure 1: Main workflow of the OSSE.

410
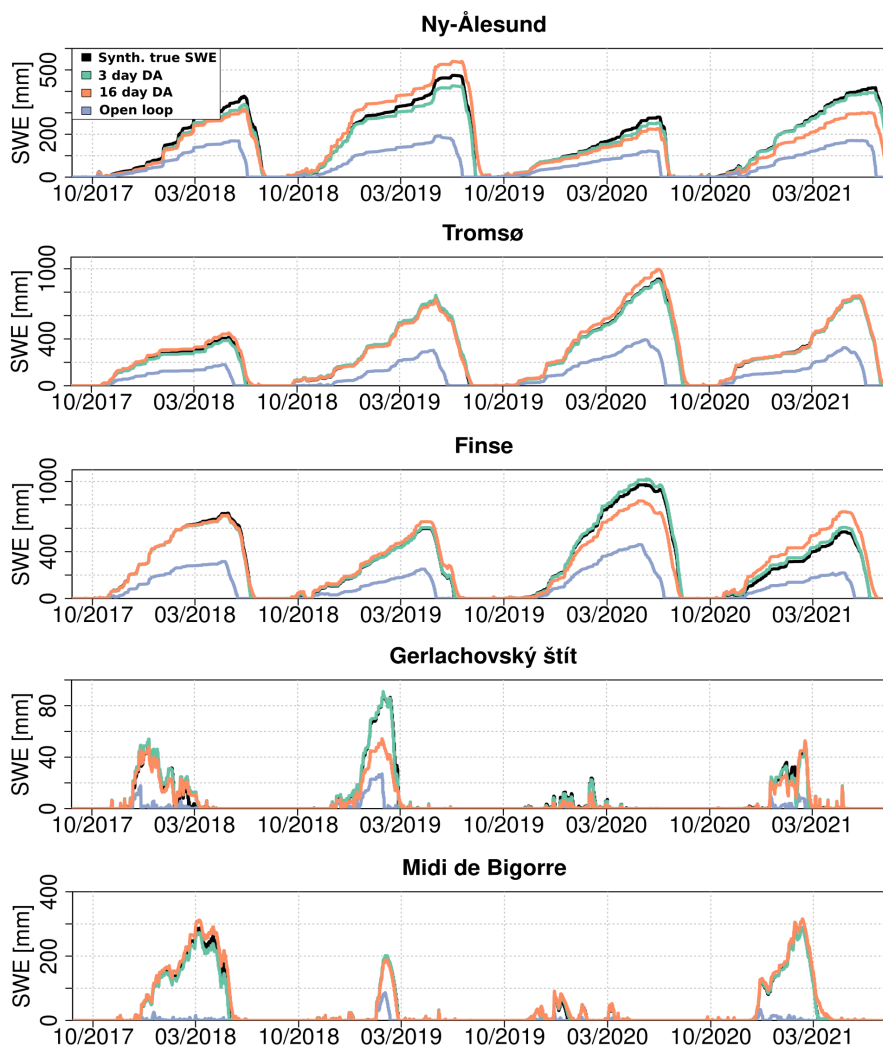
Figure 2: Comparison of hourly time series of synthetic true SWE with the open loop simulations (degraded forcing) and the posterior SWE after assimilating LST with a revisit time of 16 days or 3 days (0% cloud cover scenario) using the PBS. Here, the posterior SWE is the average of the 100 replicates.

415
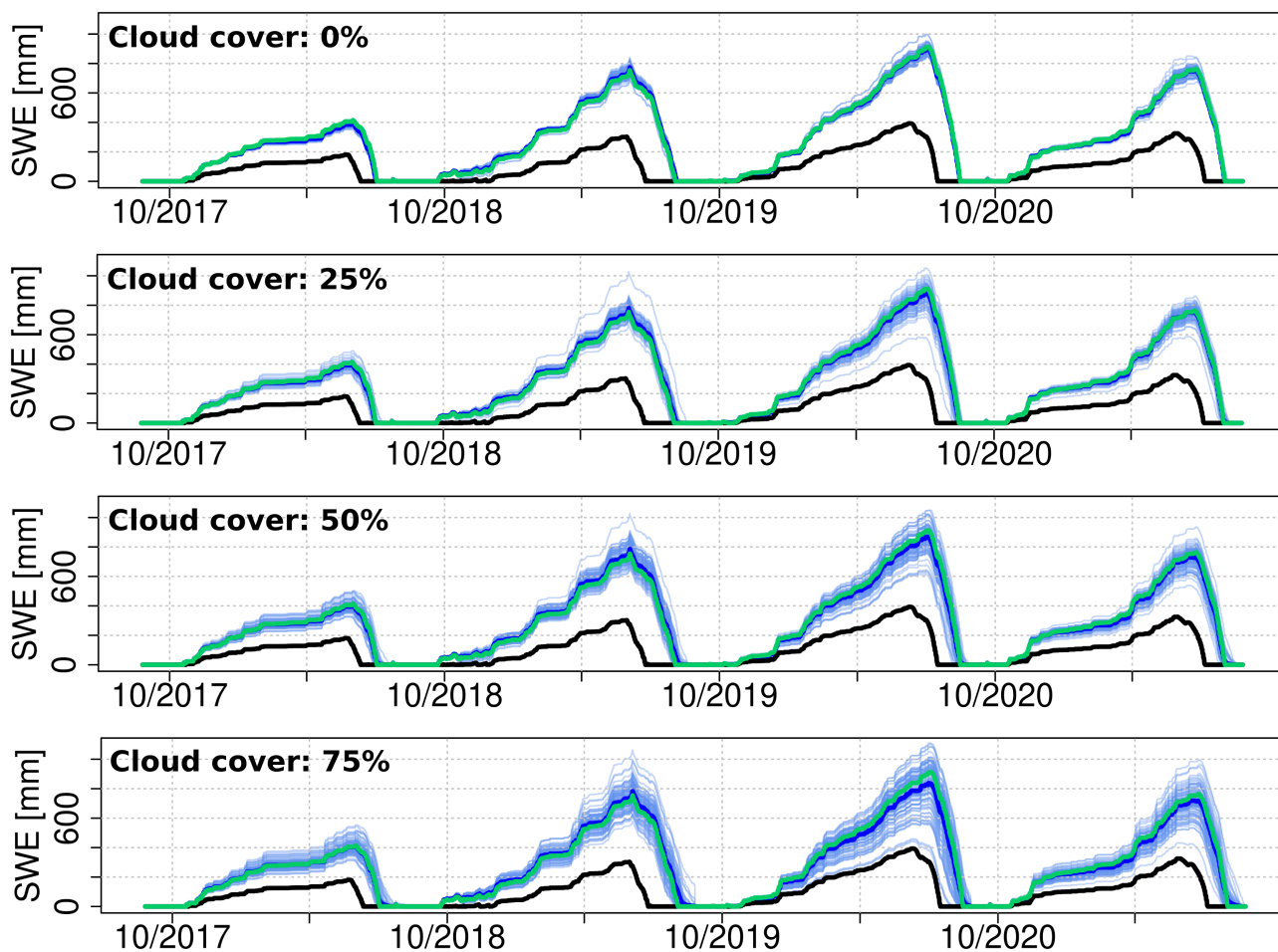
Figure 3: *Comparison of hourly time series of synthetic true SWE (green) with the open loop simulations (degraded forcing, in black), and the 100 replicates of posterior SWE after assimilating LST with a revisit time of 3 days and varying cloud cover scenarios and the* averrage *of the experiments (blue and dark blue respectivelly).*
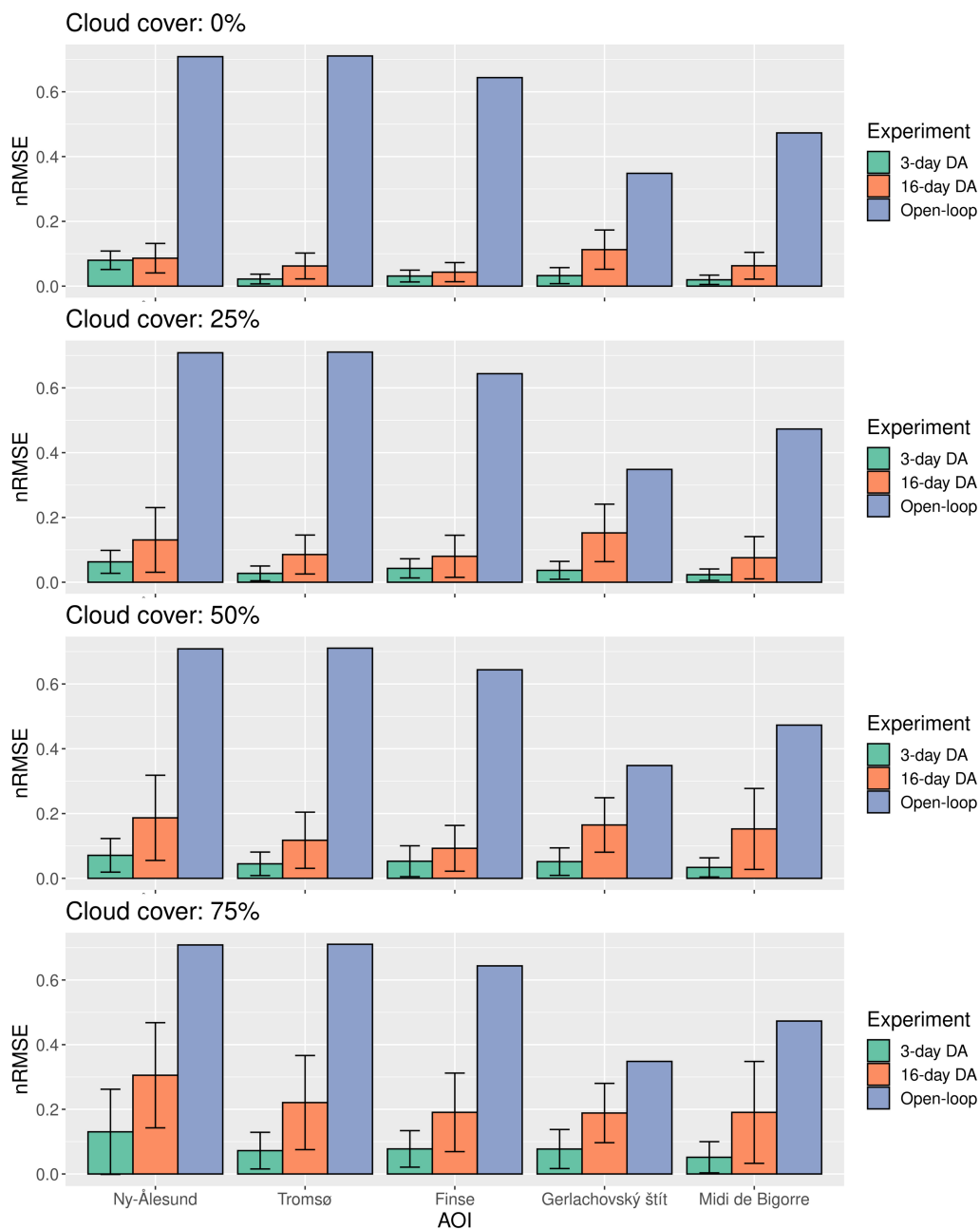
Figure 4: Normalized root mean square error (nRMSE) of the posterior SWE from the PBS compared with the synthetic true SWE for each experiment. The bars indicate the mean nRMSE while the error bars indicate the standard deviation in the 100 replicates.

420
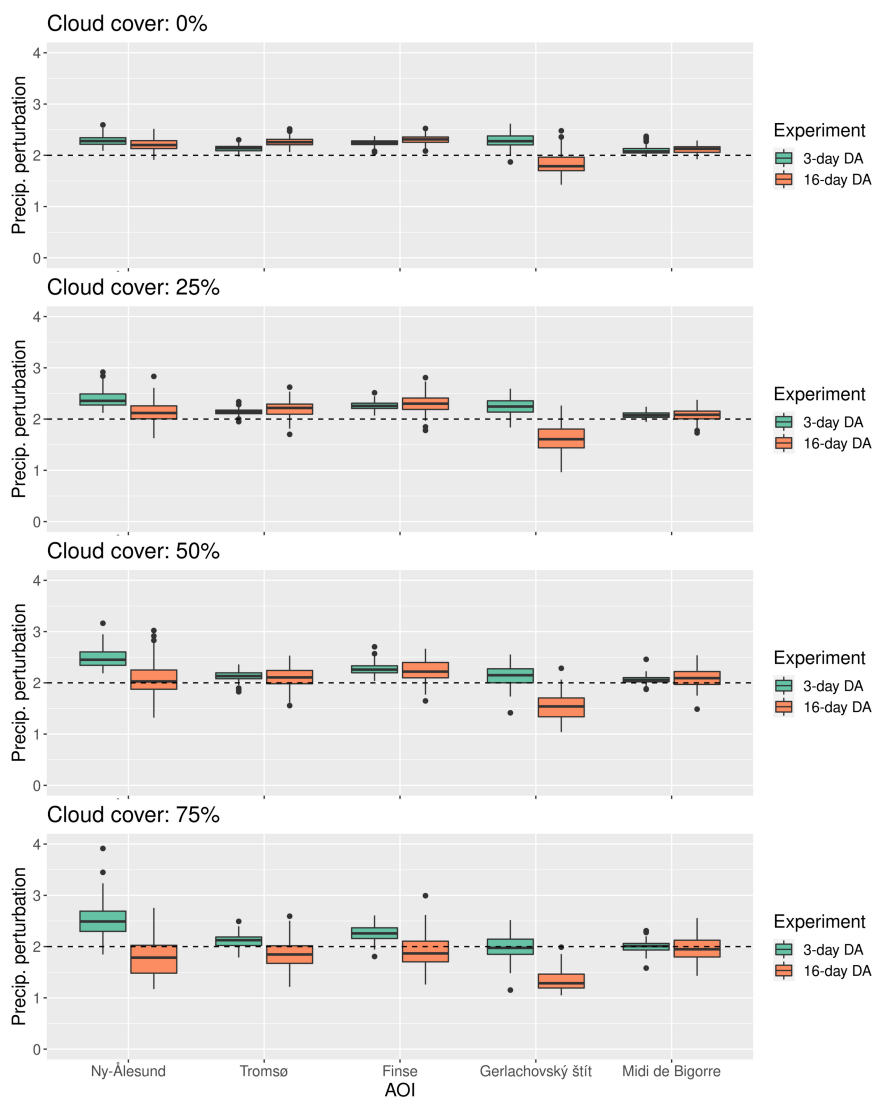
Figure 5: Boxplots showing the distribution of the posterior precipitation perturbation parameter for each experiment estimated by the PBS. The dashed line indicates the true perturbation that was applied to the forcing.
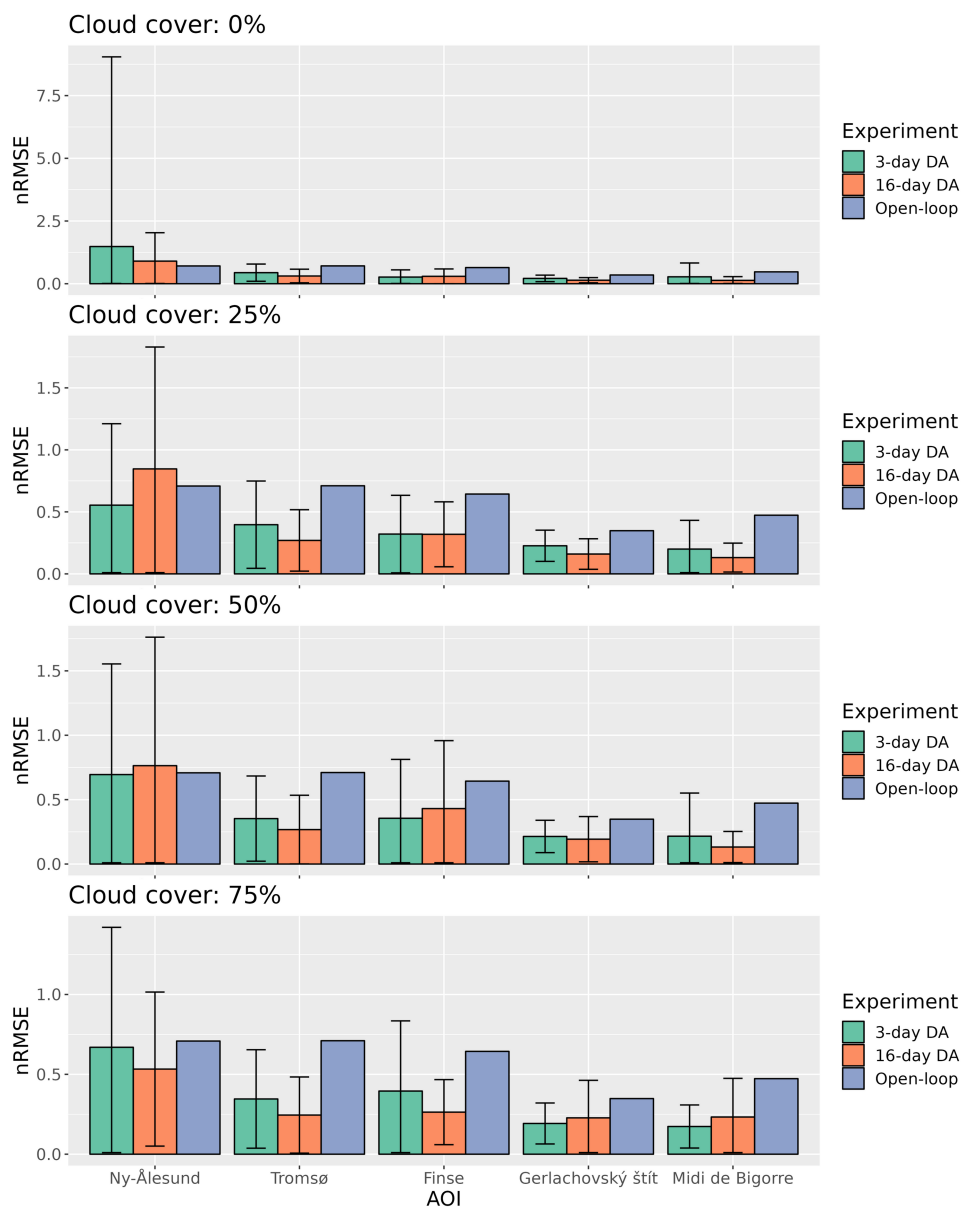
Figure 6: Boxplots showing the distribution of the posterior precipitation perturbation parameter for each experiment estimated by the PF. The dashed line indicates the true perturbation that was applied to the forcing.

425